Structure Determination of Helical Fibers by Numerical Simulation for Small-Angle Neutron Scattering†

Hiroshi Fukuda,*,‡ Ayako Goto,‡ and Toyoko Imae*,§

School of Administration and Informatics, University of Shizuoka, Yada 52-1, Shizuoka 422-8526, Japan, and Research Center for Materials Science, Nagoya University, Nagoya 464-8602, Japan

Received January 13, 2002. In Final Form: May 10, 2002

Theoretical equations for the small-angle scattering of double-strand helixes with fanlike and round cross sections, as well as a cylinder, were applied to determine the geometry of the self-assembled helical structure formed by *N*-octadecanoyl-L-aspartic acid (C_{18}Asp). However, those already-known equations were not sufficient to reproduce the experimental small-angle neutron scattering (SANS) curves. Then, a theoretical equation to the small-angle scattering for a helical fiber was derived. The equation with 5-fold integration covers the available equations for fibers with finite cross sections, but it is generalized so as to suit the multistrand helical structures with arbitrary cross-sectional shapes. Computer simulations based on this theory showed that the best fit to the observed SANS data of C_{18}Asp fiber is obtained for a model of a single-strand helix with rectangular cross section, that is, the twisted ribbon.

I. Introduction

One of the commercialized applications of amphiphiles is the utilization as gelators in organic and aqueous mediums. In many cases, fibrous assemblies are formed in gels, forming networks. The morphologies of fibers, which were determined by optical microscopy, transmission electron microscopy (TEM), and atomic force microscopy, are spiral, superhelix, cylinder, hollow tube, double tube, ribbon, platelet, cigar, and ring.[1−16] However, the thickness, length, flexibility, and cross-sectional structure are different from fibers to fibers.

The quantitative analyses of local fiber structures, such as cross-sectional shape and size, were carried out by means of small-angle X-ray scattering (SAXS) and small-angle neutron scattering (SANS). Terech and collaborators,[17] using a cylinder model under the consideration of a size distribution, analyzed the scattering data of organogels of steroid surfactants. They found that the thickness of long and rigid rods is slightly sensitive to the solvent species. They[18] carried out the analysis of organogels of 12-hydroxyoctadecanoic acid and its Li salt and found that the aggregates in xylene, hexadecane, decalin, benzene, and fluorobenzene can be described as relatively monodisperse infinitely long rigid rods with a square cross section. However, the cross-sectional structure parameters obtained from SANS for fibers in other solvents correspond to an elongated rectangular or even lamellar-like (ribbonlike) shape.

Imae et al.[13] analyzed SANS data of supramolecular fibrils formed in liquid crystals of the ternary system, azo dye/water/methanol. Since the cross-sectional radius obtained from a long rod particle model corresponds to the molecular length, a possible model of fibrils is an arrangement like rodlike micelles. An alternative model is a linear assembly of paired dyes in the antiparallel way. Small-angle scattering data of hydrogels of fluorinated-hydrogenated glucophospholipid (F-Glu) were analyzed on the basis of a theoretical equation derived for very long hollow tubules. The wall of tubules appears to consist of three bilayers of F-Glu.[12]

† This article is part of the special issue of *Langmuir* devoted to the emerging field of self-assembled fibrillar networks.

‡ University of Shizuoka.

§ Nagoya University.

(1) (a) Tachibana, T.; Kambara, H. *J. Am. Chem. Soc.* **1965**, *87*, 3015. (b) Tachibana, T.; Kitagawa, S.; Takeno, H. *Bull. Chem. Soc. Jpn.* **1970**, *43*, 2418.

(2) (a) Hidaka, H.; Miura, M.; Onai, T. *J. Chem. Soc., Chem. Commun.* **1984**, 562. (b) Hidaka, H. *Colloids Surf.* **1991**, *58*, 1.

(3) (a) Nakashima, N.; Asakuma, S.; Kim, J.-M.; Kunitake, T. *Chem. Lett.* **1984**, 1709. (b) Nakashima, N.; Asakuma, S.; Kunitake, T. *J. Am. Chem. Soc.* **1985**, *107*, 509.

(4) (a) Wade, R. H.; Terech, P.; Hewat, E. A.; Ramasseul, R.; Volino, F. *J. Colloid Interface Sci.* **1986**, *114*, 442. (b) Terech, P.; Wade, R. H. *J. Colloid Interface Sci.* **1988**, *125*, 542.

(5) (a) Fuhrhop, J.-H.; Schnieder, P.; Rosenberg, J.; Boekema, E. *J. Am. Chem. Soc.* **1987**, *109*, 3387. (b) Fuhrhop, J.-H.; Svenson, S.; Boettcher, C.; Rossler, E.; Vieth, H.-M. *J. Am. Chem. Soc.* **1990**, *112*, 4307.

(6) Yanagawa, H.; Ogawa, Y.; Furuta, H.; Tsuno, K. *Chem. Lett.* **1988**, 269. *Chem. Lett.* **1989**, 403. *J. Am. Chem. Soc.* **1989**, *111*, 4567.

(7) (a) Imae, T.; Takahashi, Y.; Muramatsu, H. *J. Am. Chem. Soc.* **1992**, *114*, 3414. (b) Imae, T.; Kidoaki, S. *J. Jpn. Oil Chem. Soc.* **1995**, *44*, 301. (c) Imae, T.; Hayashi, N.; Matsumoto, T.; Tada, T.; Furusaka, M. *J. Colloid Interface Sci.* **2000**, *225*, 285.

(8) (a) Hanabusa, K.; Okui, K.; Karaki, K.; Koyama, T.; Shirai, H. *J. Chem. Soc., Chem. Commun.* **1992**, 1371. (b) Hanabusa, K.; Matsumoto, Y.; Miki, T.; Koyama, T.; Shirai, H. *J. Chem. Soc., Chem. Commun.* **1994**, 1401.

(9) Gulik-Krzywicki, T.; Fouquey, C.; Lehn, J.-M. *Proc. Natl. Acad. Sci. U.S.A.* **1993**, *90*, 163.

(10) Bonaccio, S.; Wessicken, M.; Berti, D.; Walde, P.; Luisi, P. L. *Langmuir* **1996**, *12*, 4976.

(11) (a) Shimizu, T.; Kogiso, M.; Masuda, M. *Nature* **1996**, *383*, 487. (b) Shimizu, T.; Masuda, M. *J. Am. Chem. Soc.* **1997**, *119*, 2812.

(12) (a) Imae, T.; Krafft, M.-P.; Giulieri, F.; Matsumoto, T.; Tada, T. *Prog. Colloid Polym. Sci.* **1997**, *106*, 52. (b) Krafft, M. P.; Riess, J. G. *Biochimie* **1998**, *80*, 489. (c) Imae, T.; Funayama, K.; Krafft, M.-P.; Giulieri, F.; Tada, T.; Matsumoto, T. *J. Colloid Interface Sci.* **1999**, *212*, 330.

(13) Imae, T.; Gagel, L.; Tunich, C.; Platz, G.; Iwamoto, T.; Funayama, T. *Langmuir* **1998**, *14*, 2197.

(14) Emmanouil, V.; El Ghoul, M.; André-Barrès, C.; Guidetti, B.; Rico-Lattes, I.; Lattes, A. *Langmuir* **1998**, *14*, 5389.

(15) (a) Imae, T.; Ikeda, Y.; Iida, M.; Koine, N.; Kaizaki, S. *Langmuir* **1998**, *14*, 5631. (b) Ikeda, Y.; Imae, T.; Iida, M.; Koine, N.; Kaizaki, S. *Langmuir* **2001**, *17*, 361.

(16) Yamada, N.; Ariga, K.; Naito, M.; Matsubara, K.; Koyama, E. *J. Am. Chem. Soc.* **1998**, *120*, 12192.

(17) (a) Terech, P. *Prog. Colloid Polym. Aci.* **1990**, *82*, 263. (b) Terech, T.; Furman, I.; Weiss, R. G. *J. Phys. Chem.* **1995**, *99*, 9558.

(18) (a) Terech, P. *Colloid Polym. Sci.* **1991**, *269*, 490. *J. Phys. II France* **1992**, *2*, 2181. (b) Terech, P.; Rodriguez, V.; Barnes, J. D.; McKenna, G. B. *Langmuir* **1994**, *10*, 3406.

10.1021/la025528r CCC: $22.00
Published on Web 07/16/2002

Imae et al.[7] also reported the formation of fibrous assemblies in 1% hydrogels of *N*-acyl-L-aspartic acid (C_n-ASP, $n = 12, 14, 16, 18$) at around neutral pH and at low temperature, although the absolute pH and temperature regions depend on the alkyl chain length. The infinitely long fibrous images were visualized by TEM. The fibers have uniform diameters of 120 Å in minimum and 200 Å in maximum. Minimum and maximum are repeated with a cycle of 650 Å along a contour length, and the fibers seem to take a helical conformation. The cross-sectional radii of 22−30 Å for a rod particle model were obtained from the analysis of SANS data for C_nAsp fibers. To interpret the data, three plausible models were introduced: (a) a double strand of helical bilayer strands, (b) a superhelical structure of a helical bilayer strand, and (c) a twisted ribbon of a planar bilayer sheet. However, all these models were presented without any theoretical support.

In the present work, we report the structural analysis of fibrous assemblies of C_{18}Asp. To determine the most likely structure, theoretical SANS curves were evaluated for different models and compared with the observed data. First, defined structures, such as cylinder and single and double helixes, for which the theoretical equations are available, are applied. Then, as an extension of the given above model (c), which was originally proposed for C_nAsp fibers,[7] the theoretical small-angle scattering equation with arbitrary shape of the cross section is derived. A numerical calculation program in C++ language is introduced to resolve the 5-fold integral operation, which is universal for multistrand helical fibers. From the comparison of the calculated SANS curve with the observed one, it is deduced that model (c) is the most plausible one for C_nAsp fibers.

II. Available Analytical Equations for Small-Angle Scattering of Infinitely Long Fibers with Defined Cross Sections

(1) Cylinder with Round Cross Section. It is apparent from TEM photographs that assemblies of C_n-Asp in gels take the structure of a fiber with uniform thickness.[7] Then, the simplest model of C_nAsp fibers is a cylinder. For an infinitely long cylinder with round cross section of radius R, the small-angle scattering intensity $I(Q)$ at a momentum transfer Q is written by[19,20]

$$QI(Q) = \left(\frac{2J_1(RQ)}{RQ}\right)^2 \tag{2-1}$$

where $J_1(RQ)$ is a Bessel function. The curve calculated by using eq 2-1 is given in Figure 1a and compared with the observed data for C_{18}Asp.[7] The better fit curve was obtained for $R = 60$ Å, but it is obvious that the observed curve is not reproduced by the cylinder model. The reason for that is the omission of the possible helical conformation of the C_nAsp fibers.

(2) Double-Strand Helix with Fanlike Cross Section. Pringle and Schmidt[21] derived the equation for the small-angle scattering intensity of helical macromolecules made up of two identical coaxial helixes. The theoretical calculations based on their theory were applied to SAXS of DNA[21] and SANS of steroidal gels.[20] On a model of fanlike cross section, as seen in Figure 2a, available equations for an infinitely long helix are as below

$$QI(Q) = \sum_{n=0}^{\infty} \epsilon_n \cos^2(n\varphi/2) \frac{\sin^2(n\omega/2)}{(n\omega/2)^2} [g_n(QR,a)]^2 \tag{2-2}$$

$$g_n(QR,a) = 2R^{-2}(1 - a^2)^{-1} \int_{aR}^{R} r' J_n(Qr'(1 - q_n{}^2)^{1/2})\, dr' \tag{2-3}$$

where

$$q_n = nb/QR \quad \text{at} \quad QR \geq nb$$

$$q_n = 1 \quad \text{at} \quad QR \leq nb$$

$$b = 2\pi R/P$$

$$\epsilon_0 = 1 \quad \text{and} \quad \epsilon_n = 2 \quad \text{at} \quad n \geq 1 \tag{2-4}$$

The parameters φ, ω, R, and a are defined in Figure 2a. P is the helical pitch. If $\varphi = \pi$, the center angle of the fan is given by eq 2-5.

$$\omega = 2 \sin^{-1} \frac{r}{R} \tag{2-5}$$

Figure 1b shows the curve which was calculated with the optimum parameters: $R = 100$ Å, $r = 30$ Å, $\omega = 35°$, and $P = 1300$ (=650 × 2) Å when $a = 0$ and $\varphi = \pi$. It can be clearly seen that the calculated curve, in the Q region above 0.03 Å^{-1}, does not fit to the observed data.

(3) Single- and Double-Strand Helixes with Round Cross Section. An alternative theoretical equation for the small-angle scattering intensity of a double-strand helix was reported by Puigjaner and Subirana.[22] The double-strand helix with round cross section is situated as shown in Figure 2b, where the fiber axis is equivalent to a z axis. In this figure, r_1 and r_2 are the cross-sectional radii of the two cylinders, δ_1 and δ_2 are the distances from the fiber axis to the centers of the cross sections, and α is the angle between the two cylinders. Then the scattering intensity is described by eq 2-6

$$QI(Q) = \sum_n (a_{1n}{}^2 + a_{2n}{}^2 + 2a_{1n}a_{2n} \cos n\alpha) \tag{2-6}$$

where

$$a_{in} = J_1(\delta_i Q_\perp)\pi r_i{}^2 \frac{2J_1(r_i Q_\perp)}{r_i Q_\perp}$$

$$Q_\perp{}^2 = Q^2 - \left[\frac{2\pi n}{P}\right]^2 \tag{2-7}$$

P is the helical pitch and $Q_\perp$ is the component of Q in the $x-y$ plane. It is noted that these equations, for $\alpha = 0$, correspond to the small-angle scattering intensity of a single-strand helix.

The curve for a double-strand helix with the optimum parameters $r_1 = r_2 = r = 30$ Å, $\delta_1 = \delta_2 = \delta = 70$ Å, $\alpha = \pi$, and $P = 1300$ Å is drawn in Figure 1c, and the curve for a single-strand helix with the optimum parameters $r_1 = r_2 = r = 30$ Å, $\delta_1 = \delta_2 = \delta = 70$ Å, $\alpha = 0$, and $P = 1300$ Å is drawn in Figure 1d. Nonagreement with the observed data is observed, especially, in the lower Q region. This

(19) Vainshtein, B. K. In *Diffraction of X-rays by chain molecules*; Elsevier: New York, 1966.
(20) Terech, P.; Volino, F.; Ramasseul, R. *J. Phys.* (*Paris*) **1985**, *46*, 895.
(21) Pringle, O. A.; Schmidt, P. W. *J. Appl. Crystallogr.* **1971**, *4*, 290.
(22) Puigjaner, L. C.; Subirana, J. A. *J. Appl. Crystallogr.* **1974**, *7*, 169.

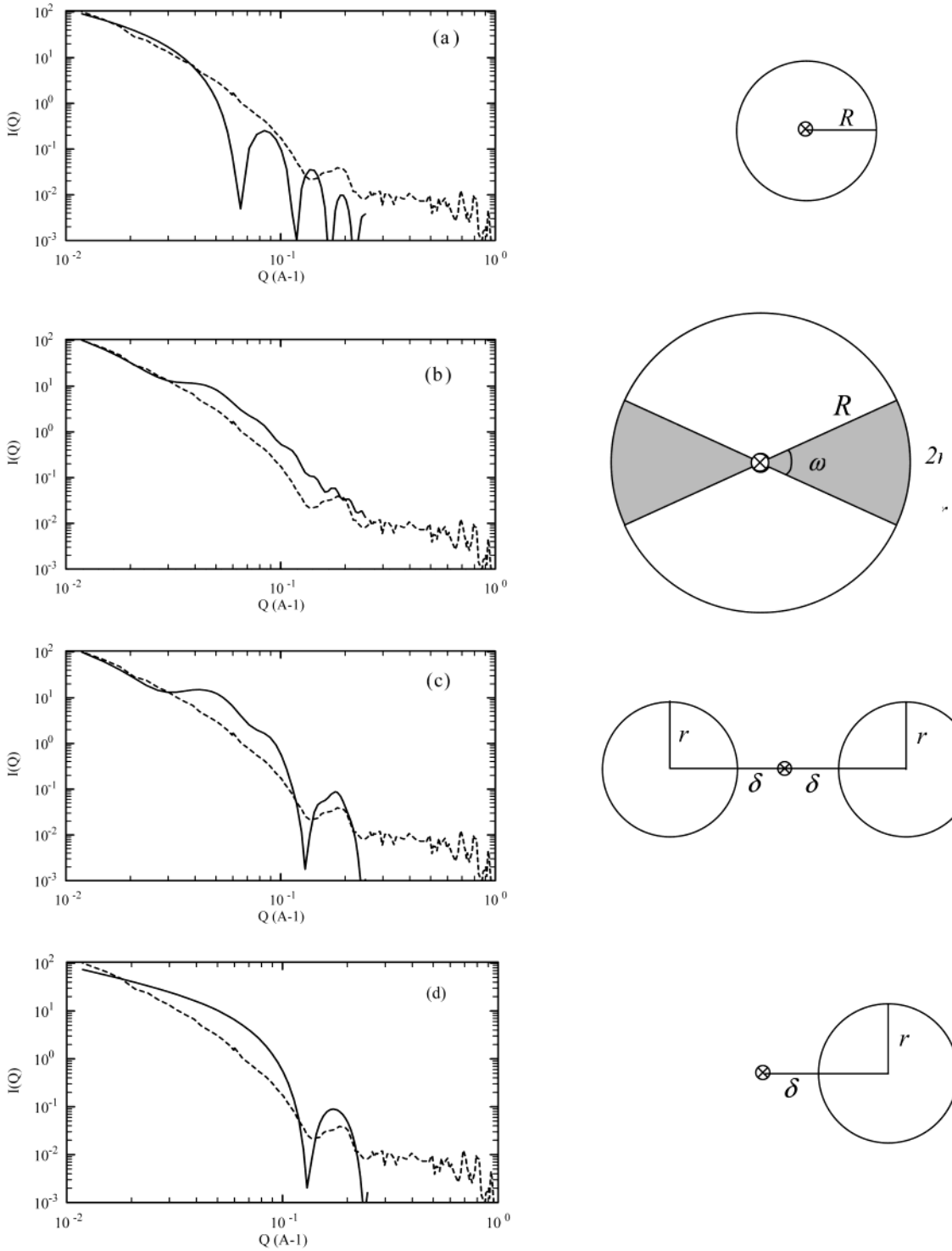

Figure 1. Comparison of model calculations using eqs 2-1, 2-2, and 2-6 and the observed SANS curve: solid line, calculated curves for (a) cylinder ($R = 60$ Å), (b) double-strand helix with fanlike cross section ($R = 100$ Å, $r = 30$ Å, $\omega = 35°$, $a = 0$, $\varphi = \pi$, $P = 1300$ Å), (c) double-strand helix with round cross section ($r_1 = r_2 = r = 30$ Å, $\delta_1 = \delta_2 = \delta = 70$ Å, $\alpha = \pi$, $P = 1300$ Å), (d) single-strand helix with round cross section ($r_1 = r_2 = r = 30$ Å, $\delta_1 = \delta_2 = \delta = 70$ Å, $\alpha = 0$, $P = 1300$ Å); broken line, observed curve for C_{18}Asp fiber in a 1 wt % aqueous solution.[7] Cross-section models are shown.

indicates that even helix models with round cross sections are not enough to interpret the structure of C_nAsp fibers.

III. Numerical Computation for Small-Angle Scattering of Infinitely Long Helical Fibers with Arbitrary Cross Sections

The single- and double-strand helixes with round cross sections as mentioned above are just the models b and a, respectively, which are two of the three plausible models introduced to explain the structure of C_nAsp fibers. Since both helical models were found to be inadequate, the other model (c) has been examined. However, since theoretical equations for model (c) are not available, the corresponding equation must be first derived. We introduce here the universal equation for the small-angle scattering of a multistrand helix with arbitrary cross sections.

For deriving a general equation of the scattering intensity from helical fibers, the geometry of the cross

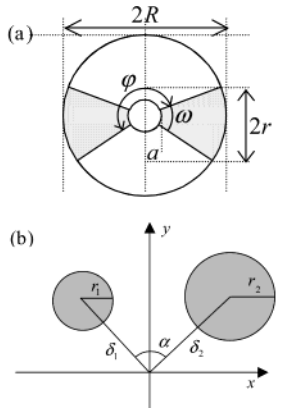

Figure 2. Geometry of the cross section of a double-strand helical fiber in the $x-y$ plane of Cartesian coordinates: (a) fanlike cross section; (b) round cross section.

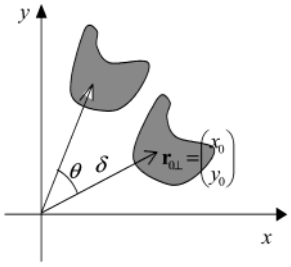

Figure 3. Geometry of the cross section of a fiber in the $x-y$ plane of Cartesian coordinates.

section in the $x-y$ plane is defined as shown in Figure 3. The coordinate (x_0,y_0) of an origin of the cross section of a fiber is located at distance δ from the main axis z of the helical fiber. Since the cross section with an arbitrary shape rotates at a pitch P around the helix axis, a matrix $R(\theta)$, as it is given in eq 3-1, is used for the transfer of the rotational angle θ in the $x-y$ coordinate

$$R(\theta) = \begin{pmatrix} \cos\theta & -\sin\theta \\ \sin\theta & \cos\theta \end{pmatrix} \tag{3-1}$$

where

$$\theta = 2\pi z/P \tag{3-2}$$

The scattering intensity $I_1(\mathbf{Q})$ of a fiber is described by a Fourier transform of the scattering length density $\rho(\mathbf{r})$ in real space. Then

$$I_1(\mathbf{Q}) = |A(\mathbf{Q})|^2 \tag{3-3}$$

$$A(\mathbf{Q}) = \int \mathrm{d}\mathbf{r}\, \rho(\mathbf{r}) \mathrm{e}^{i\mathbf{Q}\mathbf{r}} \tag{3-4}$$

where a momentum transfer vector $\mathbf{Q}$ and a position vector $\mathbf{r}$, respectively, are written by

$$\mathbf{Q} = (Q_x,Q_y,Q_z) = (\mathbf{Q}_\perp,Q_z) \tag{3-5}$$

$$\mathbf{r} = (x,y,z) = (\mathbf{r}_\perp,z) \tag{3-6}$$

When the position vector of an origin of the cross section is $\mathbf{r}_0$

$$\mathbf{r}_0 = (x_0,y_0,z_0) = (\mathbf{r}_{0\perp},z_0) \tag{3-7}$$

the scattering length density for a fiber of length L is

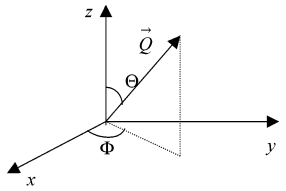

Figure 4. Notation of Q in Cartesian coordinates.

divided into two terms and described by

$$\rho(\mathbf{r}) = \rho_\perp(R(-\theta)\mathbf{r}_\perp - \mathbf{r}_{0\perp})\Pi(z,L) \tag{3-8}$$

where $\rho_\perp(x,y)$ is the scattering length density from the origin (x_0,y_0) on the $x-y$ plane and

$$\Pi(z,L) = 1 \quad \text{for} \quad |Z| \le L/2$$
$$= 0 \text{ for otherwise} \tag{3-10}$$

When substituting eq 3-8 into eq 3-4 and replacing the integral variable $\mathbf{r}_\perp$ to $R(-\theta)\mathbf{r}_\perp - \mathbf{r}_{0\perp}$, we obtain

$$A(\mathbf{Q}) = \int \mathrm{d}\mathbf{r}_\perp \rho_\perp(\mathbf{r}_\perp) \mathrm{e}^{iR(\theta)\mathbf{Q}_\perp\cdot(\mathbf{r}_\perp+\mathbf{r}_{0\perp})} \int \mathrm{d}z \Pi(z,L) \mathrm{e}^{iQ_z z} \tag{3-11}$$

The scattering intensity $I_{\mathrm{en}}(Q)$ for an ensemble of randomly dispersed fibers in a system is obtained by space-averaging the scattering intensity of a fiber $I_1(\mathbf{Q})$, according to the geometry illustrated in Figure 4, where

$$\mathbf{Q}_\perp = \begin{pmatrix} Q\sin\Theta\cos\Phi \\ Q\sin\Theta\sin\Phi \end{pmatrix} \tag{3-12}$$

$$Q_z = Q\cos\Theta \tag{3-13}$$

The resulting scattering intensity is

$$I_{\mathrm{en}}(Q) = \frac{1}{4\pi}\int_0^{2\pi} \mathrm{d}\Phi \int_0^{\pi} \sin\Theta\, \mathrm{d}\Theta |I_1(\mathbf{Q})|^2$$
$$= \frac{1}{4\pi}\int_0^{2\pi} \mathrm{d}\Phi \int_0^{\pi} \sin\Theta\, \mathrm{d}\Theta \Big| \int \times$$
$$\rho_\perp(\mathbf{r}_\perp) \mathrm{e}^{iR(\theta)\mathbf{Q}_\perp\cdot(\mathbf{r}_\perp+\mathbf{r}_{0\perp})}\, \mathrm{d}\mathbf{r}_\perp \int_{-L/2}^{L/2} \mathrm{e}^{iQ_z z}\, \mathrm{d}z \Big|^2 \tag{3-14}$$

We rewrite the scattering intensity (3-14) to a more convenient form for numerical calculation making the range of the z integral independent of the length L of the fiber. Since $R(\theta)$ is a periodic function of a period 2π, if we describe the length of a fiber by

$$L = mP \tag{3-15}$$

where m is an odd integer, we obtain the following expression for the scattering intensity

$$I(Q;m) = \frac{1}{4\pi mP}\int_0^{2\pi} \mathrm{d}\Phi \int_0^{\pi} \sin\Theta\, \mathrm{d}\Theta |c_m(PQ_z) \int \times$$
$$\rho_\perp(x,y) \mathrm{e}^{iR(\theta)\mathbf{Q}_\perp\cdot(\mathbf{r}_\perp+\mathbf{r}_{0\perp})}\, \mathrm{d}x\, \mathrm{d}y \int_{-P/2}^{P/2} \mathrm{e}^{iQ_z z}\, \mathrm{d}z \Big|^2 \tag{3-16}$$

where

$$c_m(PQ_z) = 1 + 2\cos PQ_z + \cdots + 2\cos\frac{m+1}{2} PQ_z \tag{3-17}$$

Hence, for infinitely long fibers we obtain

$$I_{\mathrm{inf}}(Q) = \lim_{m\to\infty} I(Q;m) \tag{3-18}$$

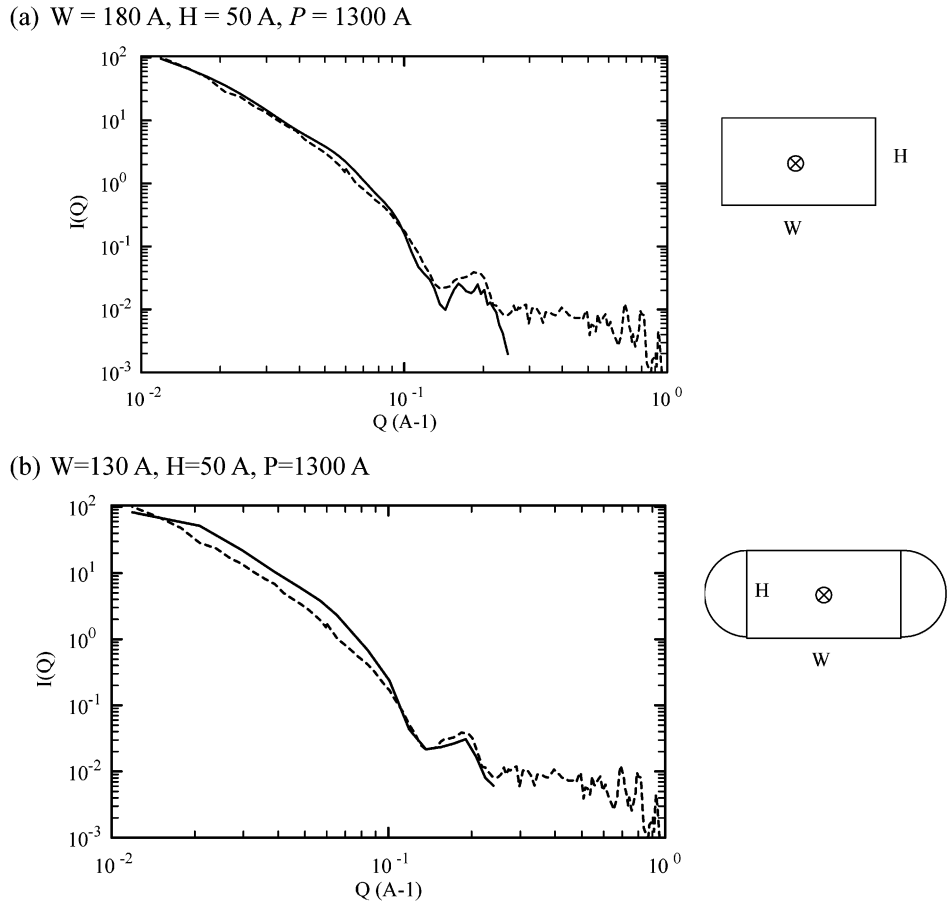

Figure 5. Comparison of model calculations using a 5-fold integral equation for a twisted ribbon and the observed SANS curve: solid line, calculated curves for (a) single-strand helix with rectangular cross section (W = 180 Å, H = 50 Å, P = 1300 Å), (b) single-strand helix with edge-covered rectangular cross section (W = 130 Å, H = 50 Å, P = 1300 Å); broken line, observed curve for C_{18}Asp fiber in a 1 wt % aqueous solution.[7] Cross-section models are shown.

For the scattering intensity of multistrand helical fibers, $\rho_\perp(x,y)$ is described as a sum of the cross-section components of the fiber. The shape of the cross section is alterable by the integrand of x and y, that is, $\rho_\perp(x,y)$.

The 5-fold integrals of Φ, Θ, x, y, and z in the finite range given by eq 3-16 can be calculated according to the Gauss−Legendre method.[23] For a numerical calculation, it is convenient to define $\rho_\perp(x,y)$ of the helix by the inheritance of the class in C++ language. We defined the following "section_list" class in C++ language and then any $\rho_\perp(x,y)$ from the origin (x_0,y_0) by the inherited classes of it.

```
class section_list
{
protected:
  static double Q; //momentum transfer
  double QRx() const; // x component of R(θ)Q⊥ in eq 3-16
  double QRy() const; // y component of R(θ)Q⊥ in eq 3-16
  cmplx expxy(double x, double y) const; // e^{iQ⊥r⊥} in eq 3-16
public:
  double x0,y0; // origin of the cross section from the axis of the helix (x0,y0)
  void add(); // add the cross section to the helix
  virtual inline cmplx figure() const =0; // define cross section
};
```

Small-angle scattering curves for double-strand helixes calculated using the theoretical equation derived above were compared with those from available equations (2-2) and (2-6). Model calculations with $m = 7$ and the same geometrical parameters of fibers were perfectly consistent with those from latter ones, which is shown in Figure 1, for helixes with fanlike and round cross sections. This indicates that the derived equation is exactly equivalent to the available equations already reported, if we use sufficiently large m. In fact, for $m = 7$, the length of helical object $L = 7 \times 1300$ Å is sufficiently large compared with the cross-sectional radius of object, several tenths Å.

IV. Helical Fiber Self-Assembled by Amino Acid Surfactant

As discussed above, it is doubtful that the single and double strands of helical bilayer strands (models (b) and (a)), modeled as single- and double-strand helixes with round cross sections, respectively, are adequate models for C_nAsp fibers. Then, the equation (3-16) derived was applied to the model (c) of a twisted ribbon. A twisted ribbon of a planar bilayer sheet (model (c)) can be regarded as a single-strand helix with rectangular cross section. A computer simulation was then carried out on the basis of this model, and the corresponding small-angle scattering curves, calculated with the optimum parameters, were compared with the observed SANS curve of C_{18}Asp fibers,[7] as shown in Figure 5a. The fitting to the observed curve is the best for the calculation based on a single-strand helix with rectangular cross section with the following

(23) Abramowitz, M.; Stegun, I. A. *Handbook of mathematical functions*; Dover Publications: New York, 1970.

W=180 A, H=40 A, P=1300 A

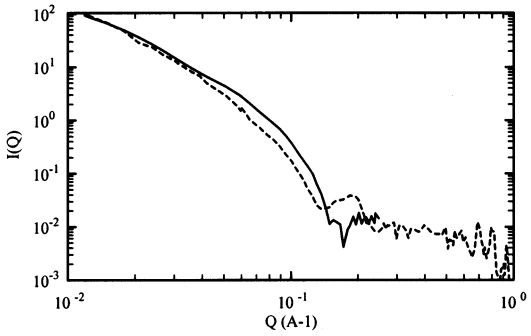

W=180 A, H=45 A, P=1300 A

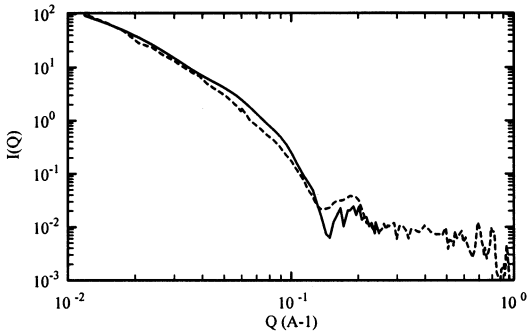

W=180 A, H=50 A, P=1300 A

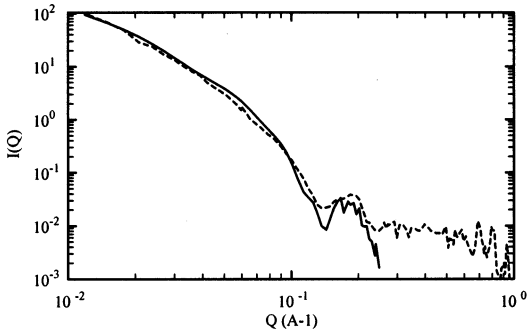

Figure 6. Comparison of model calculations using a 5-fold integral equation for a twisted ribbon and the observed SANS curve: solid line, calculated curves as a variation of short width of rectangular cross section; broken line, observed curve for C_{18}Asp fiber in a 1 wt % aqueous solution.[7] Used parameters are given in the figure.

W=200 A, H=50 A, P=1300 A

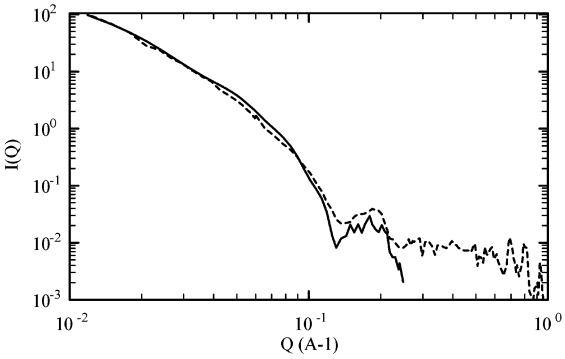

W=180 A, H=50 A, P=1300 A

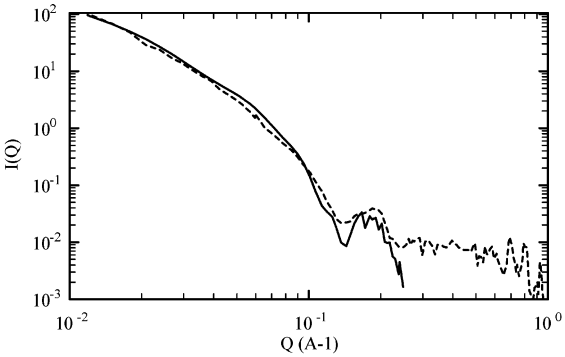

W=160 A, H=50 A, P=1300 A

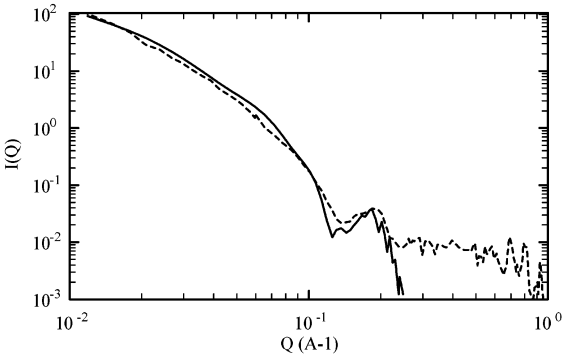

Figure 7. Comparison of model calculations using a 5-fold integral equation for a twisted ribbon and the observed SANS curve: solid line, calculated curves as a variation of long width of rectangular cross section; broken line, observed curve for C_{18}Asp fiber in a 1 wt % aqueous solution.[7] Used parameters are given in the figure.

parameters: long width $W = 180$ Å, short width $H = 50$ Å, and helical pitch $P = 1300$ Å. Since the good fitting spans now to regions of up to $Q = 0.2$ Å^{-1}, it is concluded that the helical ribbon is the best model of C_nAsp fibers.

The effect of the variation of the parameters was examined, and this can be seen in Figures 6−8. As the short width of rectangular cross section is shortened from 50 to 40 Å, the $I(Q)$ vs Q curve becomes more gradual and a peak at around $Q = 0.02$ Å^{-1} shifts to larger Q values (see Figure 6). This tendency is consistent with that observed in SANS curves for C_{18}Asp to C_{14}Asp fibers.[7] If the rectangular cross section is formed by bilayers, the short width must be the double of the molecular length. Since the calculated molecular lengths of C_nAsp ($n = 14$, 16, 18) are 22.5, 25.0, and 27.5 Å, respectively,[7] the double of their lengths is consistent with the variation of the short width, if the alkyl chains are slightly tilted or melted. Figure 7 shows the effect of the long width in rectangular cross section. Even if the width is changed from 160 to 200 Å, the calculated intensity curves are scarcely affected. This suggests that the size distribution of long widths is insensitive to the scattering curves. Similar conclusions were obtained for the helical pitch. As it is seen in Figure 8, the changes of the helical pitch in the range 1100−1300 Å, which is within the observed error, give a meaningless influence to the scattering curves.

Upon the basis of the numerical simulation, it is then considered that the twisted ribbon model, that is, the single-strand helix with rectangular cross section, is the best fitted model for the C_nAsp fibers, in which the cross section of the ribbon consists of a bilayer of the component molecules. However, this twisted ribbon is not reasonable from the viewpoint of a self-assembly structure, because the alkyl chains in the edge of the bilayer are exposed to

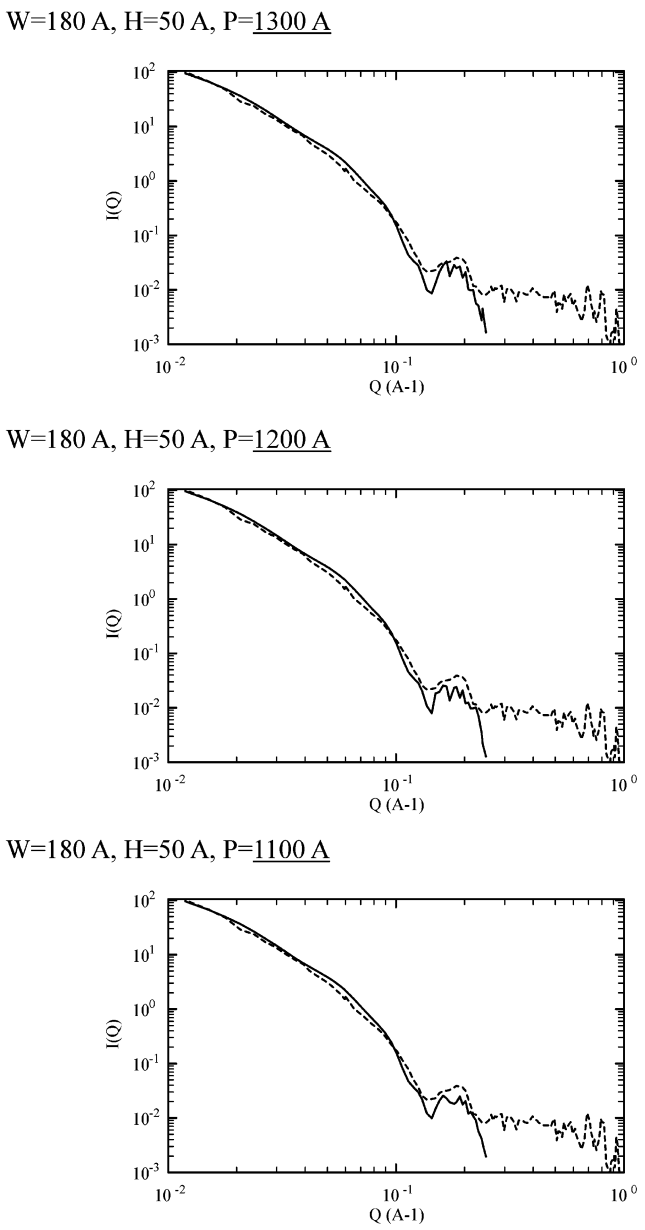

Figure 8. Comparison of model calculations using a 5-fold integral equation for a twisted ribbon and the observed SANS curve: solid line, calculated curves as a variation of helical pitch; broken line, observed curve for C_{18}Asp fiber in a 1 wt % aqueous solution.[7] Used parameters are given in the figure.

bulk water. Therefore, another model was proposed, as shown in Figure 5b. In this case two semicircular assemblies of component molecules are attached on both edges to the ribbon in order to inhibit the direct contact of the alkyl chains with the bulk water. According to this model with edge-covered rectangular cross section, the fitting curve was drawn and it is shown in Figure 5b. Since the fitting curve deviates slightly in the region of small *Q*, this model does not seem to be the most plausible one considering the self-assembly of the fibers. It was reported that bilayer ribbon's edges are different from the entire ribbon surface in the character and the twisted bilayer ribbons close to yield tubles.[24] This supports the rectangular cross section without covered edges as determined above.

After all, an optimum model for the C_{18}Asp fibers is as shown in Figure 9. In the comparison with the observation

(24) Goren, M.; Qi, Z.; Lennox, B. *Chem. Mater.* **2000**, *12*, 1220.

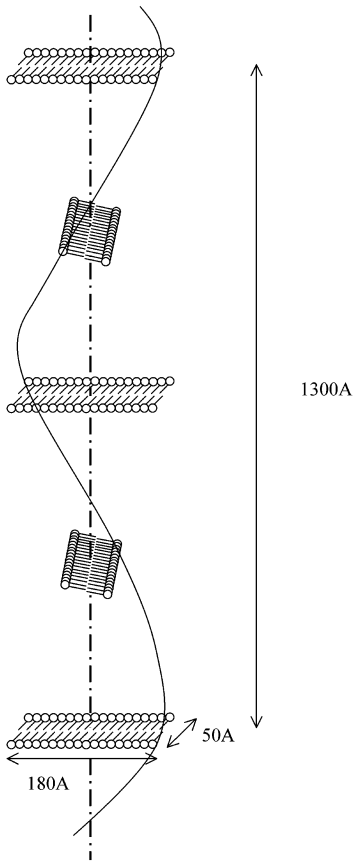

Figure 9. An optimum model for a C_{18}Asp fiber.

by TEM, the helical pitch of a twisted ribbon is double that of the observed cycle of minimum and maximum along a contour length of a fiber. The long width of the planar bilayer sheet in the cross-sectional area of a ribbon is consistent with the maximum diameter of C_{18}Asp fibers. However, the short width, which is double the molecular length, is not in agreement with the observed minimum diameter. This fact results from the resolution of TEM. That is, in the accumulation of twisted monolayers with about 5 Å thickness and 50 Å short width, the minimum width is difficult to resolve by TEM.

V. Conclusions

The available theoretical equations so far for small-angle scattering of fibers were separately introduced for different kinds of structures. One inconvenience for utilizing them is the separate programming, when the different structures are compared. Other demerit is that its use is limited to structures where the theoretical equations are available. Theoretical analyses for double-strand helix models were carried out using the available equations. However, such trial did not succeed to reproduce the SANS curves of C_nAsp fibers. As the single-strand helix is another possibility for modeling C_nAsp fibers, the corresponding theoretical equations were derived in this work.

Since the strict equation for the calculation consists of a 5-fold integral equation, the calculation is troublesome. However, if one programs at once the universal equation, this program can be used for the calculation of the small-angle scattering of fibers with any kind of cross-sectional shape. The equation can be used even for a multistrand

helix and also for a helix with inhomogeneous scattering length. From the application of this equation to C_nAsp fibers, it was concluded that the fibers must be twisted ribbons. The cross section of ribbons consists of a bilayer of the component molecules, the width being three to four times larger than the bilayer thickness.

Acknowledgment. We thank for Mr. Yingqun Fang and Ms. Hiroko Tanaka for their help with the numerical computation.

LA025528R